Improvement of Quasi-Monostatic Frequency-Swept Microwave Imaging of Conducting Objects Using Illumination Diversity Technique

Chao-Hsiung Tseng, *Member, IEEE*, and Tah-Hsiung Chu, *Member, IEEE*

***Abstract*—In this paper, a quasi-monostatic frequency-swept microwave imaging system using illumination diversity technique is proposed to have an efficient scattered field acquisition arrangement. The measurement system, calibration method, and experimental results are presented. The image reconstruction principle is developed under physical optics approximation. Reconstructed images of the continuous, discrete conducting objects and B-52 model aircraft measured in the frequency range 7.5–12.5 GHz are shown to be in good agreement with the scattering object geometries. The images reconstructed with and without using illumination diversity technique are presented to illustrate the effectiveness of the developed microwave imaging system.**

***Index Terms*—Electromagnetic scattering, microwave imaging, microwave measurements.**

I. Introduction

THE theory of monostatic microwave imaging for perfectly conducting objects based on Bojarski's identity was described in [1], [2]. For image resolution improvement, the frequency and angular diversity techniques [3], [4] are adopted to enlarge the area of scattering object Fourier-domain data. In the monostatic scattering arrangement, or inverse synthetic aperture radar (ISAR) [5], the frequency-swept object scattering information is acquired by rotating the scattering object at the corresponding transmitting/receiving direction, then recording the object scattered far field in a sequential format. In other words, a line of Fourier-domain data corresponding to one object rotation angle is acquired using frequency diversity technique, and a two-dimensional (2-D) polar format of the object Fourier-domain data is obtained by using angular diversity technique.

Under the physical optics approximation [6], [7], the theory based on Bojarski's identity was extended to the general multistatic case [8]. In this arrangement, the scattering object is illuminated by a single source and the scattered far field is recorded by multiple receivers (i.e., receiver diversity technique). Namely, multiple lines of Fourier-domain data are obtained using the receiver diversity technique at one object rotation angle. Compared with the monostatic scattering arrangement for a stationary scatterer, its image angular resolution is improved and the Fourier-domain data are acquired more efficiently. However, it may increase the system cost due to the increased number of coherent receivers.

In this paper, the quasi-monostatic frequency-swept microwave imaging using illumination diversity technique is developed under the physical optics approximation. In this arrangement, a receiving antenna is exploited to simultaneously receive the scattered field contributed from multiple sources (i.e., illumination diversity technique). In the multiple illumination arrangement, one can use an N-way power divider to distribute the illumination signal to a number of transmitting antennas. It is then more cost-effective than the receiver diversity technique. In addition, it will be shown that multiple lines of the object Fourier-domain data contributed from multiple sources can be obtained at one object rotation angle; hence it can improve the image angular resolution or equivalently reduce the object rotation angles. Another approach to implement illumination diversity is to adopt the arrangement with a 1-to-n switch connected to n transmitting antennas [9]. Each antenna is given its time slot for transmitting and only one antenna is turned on in this time slot.

In the following, the formulations on image reconstruction of conducting objects using illumination diversity technique are presented in Section II. Since the scattering object is illuminated by multiple sources simultaneously, the induced surface currents contributed from each source are then coherently superimposed on the object surface. The recorded object scattered field is therefore a coherent summation of the scattered fields from all the illuminated regions. In this section, an image reconstruction method is developed to use sets of equations to solve the corresponding portion of scattered field contributed from each source. It then gives multiple lines of the object Fourier-domain data. Therefore, with the use of illumination diversity technique, it can improve the imaging angular resolution and reduce the object rotation angles effectively.

The developed microwave imaging system and calibration method for multisource illumination are described in Section III. Based on the image reconstruction method given in Section II, the calibration formulations are described to obtain the calibrated Fourier-domain data contributed from each source from the measured scattered field using multisource illumination.

In Section IV, the reconstructed images for three different types of scattering objects, including continuous, discrete line objects and B-52 model aircraft, measured in the frequency range of 7.5–12.5 GHz, are shown in good agreement with

Manuscript received January 24, 2003; revised March 19, 2004. This work was supported in part by the National Science Council of Taiwan, R.O.C., under Grant 92-2213-E-002-071, 93-2752-E-002-003-PAE and in part by the Ministry of Education of Taiwan, R.O.C., under Grant 89-E-FA06-2-4-6.

The authors are with the Graduate Institute of Communication Engineering, National Taiwan University, Taipei, Taiwan, R.O.C. (e-mail: chtseng@ew.ee.ntu.edu.tw; thc@ew.ee.ntu.edu.tw).

Digital Object Identifier 10.1109/TAP.2004.838787

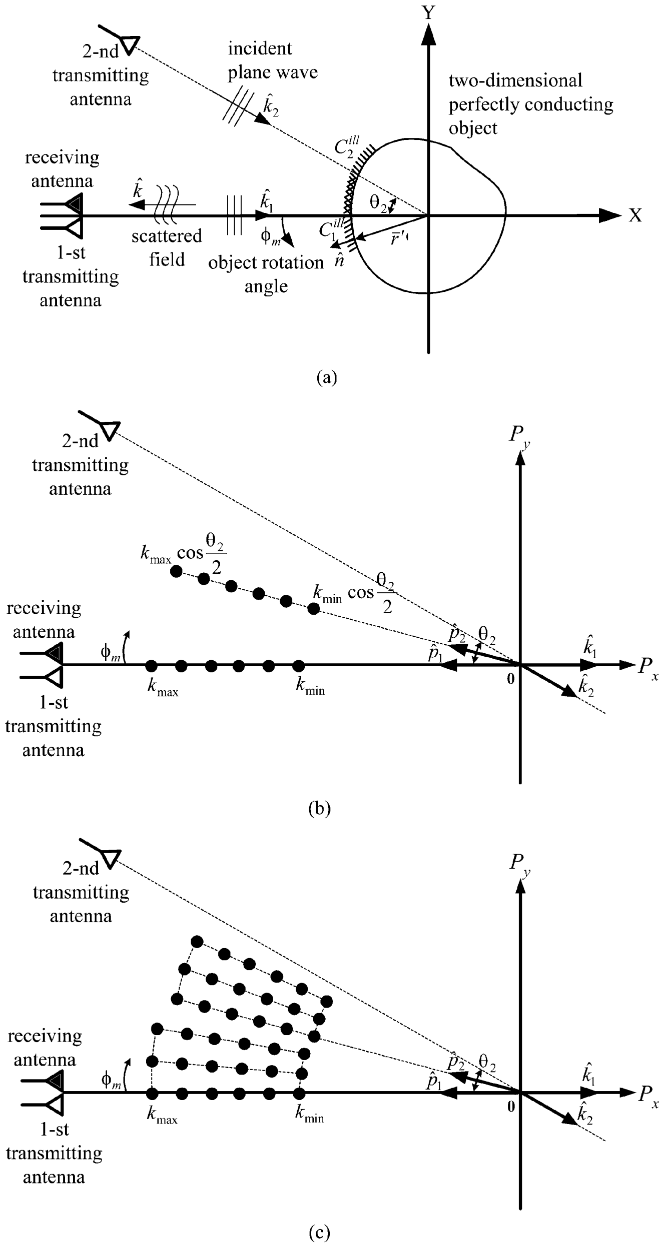

Fig. 1. (a) Two-dimensional quasi-monostatic backscattering geometry using two-source illumination and its frequency-swept Fourier-domain (b) without and (c) with object rotation.

the scattering object geometries. The comparison of images reconstructed with and without using illumination diversity technique are presented to illustrate the developed microwave imaging system to be an effective approach as compared with the monostatic arrangement.

II. Principle

The quasi-monostatic backscattering geometry using illumination diversity technique is shown in Fig. 1(a). Note, only two-source illumination is shown for the simplicity of illustration. In the following derivation, an infinitely long scattering object in the z-direction (normal to the x-y plane) is assumed and multiple normally incident TM-polarized plane waves are generated by multiple transmitting antennas in the far-field region.

The incident field for multisource illumination is written as

$$\begin{aligned}\bar{E}^i(\bar{r}) &= \hat{z}E_1 e^{-jk_0\hat{k}_1\cdot\bar{r}} + \hat{z}E_2 e^{-jk_0\hat{k}_2\cdot\bar{r}} + \cdots + \hat{z}E_n e^{-jk_0\hat{k}_n\cdot\bar{r}}\\ &= \sum_{i=1}^{n}\hat{z}E_i e^{-jk_0\hat{k}_i\cdot\bar{r}}\end{aligned} \tag{1}$$

$$\bar{H}^i(\bar{r}) = \frac{1}{\eta}\sum_{i=1}^{n}\hat{k}_i\times\hat{z}E_i e^{-jk_0\hat{k}_i\cdot\bar{r}} \tag{2}$$

where $k_0=\omega/c$ is the wave number and $\hat{k}_i$ is the direction of the ith incident plane wave. E_i is the complex field amplitude of the ith incident plane wave. η is the intrinsic impedance in free space and time dependence $\exp(jwt)$ is implied.

Assuming that the angle between the ith transmitting antenna and the receiving antenna fulfills the physical optics approximation [6], the scattered field contributed from multiple sources at the receiving antenna is given as [7]

$$\begin{aligned}\bar{E}^s = -jk_0\sum_{i=1}^{n}\int_{C_i^{\text{ill}}} & 2\hat{n}(\bar{r}')\\ & \times(\hat{k}_i\times\hat{z})E_i e^{-jk_0\hat{k}_i\cdot\bar{r}'}G(|\bar{r}-\bar{r}'|)d\bar{r}'\end{aligned} \tag{3}$$

where C_i^{ill} is the illuminated object contour contributed from the ith source. $\hat{n}(\bar{r}')$ is the outward unit normal vector of C_i^{ill} at $\bar{r}'$ and

$$G(|\bar{r}-\bar{r}'|) = \frac{e^{-j\bar{k}\cdot(\bar{r}-\bar{r}')}}{|\bar{r}-\bar{r}'|} \tag{4}$$

is the Green's function in free space. $\bar{k}=k_0\hat{k}$ and $\hat{k}$ is the direction of receiving antenna.

As the polarization of receiving antenna is in the z-direction, the scattered field in the far-field region becomes

$$\begin{aligned}U^s &= \hat{z}\cdot\bar{E}^s\\ &= -jk_0\sum_{i=1}^{n}E_i\int\int O_i(\bar{r}')e^{-jk_0\hat{k}_i\cdot\bar{r}'}\\ &\quad\cdot\frac{e^{-j\bar{k}\cdot(\bar{r}-\bar{r}')}}{|\bar{r}-\bar{r}'|}d^2\bar{r}'\end{aligned} \tag{5}$$

$$\begin{aligned}&\approx\frac{-jk_0e^{-jk_0r}}{r}\\ &\quad\cdot\sum_{i=1}^{n}E_i\int\int O_i(\bar{r}')e^{-jk_0(\hat{k}-\hat{k}_i)\cdot\bar{r}'}d^2\bar{r}'\end{aligned} \tag{6}$$

where

$$O_i(\bar{r}') = 2\hat{n}(\bar{r}')\cdot\hat{p}_i\delta(C_i(\bar{r}')) \tag{7}$$

is defined as the partial microwave image contributed from the ith source and is related to the object shape. $\hat{p}_i$ is the unit wave vector defined as $\hat{p}_i=(\hat{k}-\hat{k}_i)/|\hat{k}-\hat{k}_i|$. $\delta(C_i(\bar{r}'))$ is a one-dimensional (1-D) Dirac delta function corresponding to the ith source with its argument defined as

$$C_i(\bar{r}')\begin{cases}=0, & \text{as } \bar{r}'\in C_i^{\text{ill}}\\ \neq 0, & \text{elsewhere.}\end{cases} \tag{8}$$

By defining the Fourier transformation of $O_i(\bar{r}')$ as

$$\tilde{O}_i(\bar{p}_i) = \int\int O_i(\bar{r}')e^{j\bar{p}_i\cdot\bar{r}}d^2\bar{r}. \tag{9}$$

Equation (6) can be expressed as

$$U^s = C_R \sum_{i=1}^{n} E_i \tilde{O}_i(\bar{p}_i) \tag{10}$$

where C_R is the range-related term $(-jk_0 e^{-jk_0 r}/r)$. $\bar{p}_i$ is

$$\begin{aligned}\bar{p}_i &= k_0 \cos\frac{\theta_i}{2}\hat{p}_i \\ &= k_0 \cos\frac{\theta_i}{2}(\sin\phi_m \hat{p}_x + \cos\phi_m \hat{p}_y).\end{aligned} \tag{11}$$

$\bar{p}_i = p_{ix}\hat{p}_x + p_{iy}\hat{p}_y$ is the wave vector in object Fourier-domain space, i.e., $\bar{p}$-space. θ_i is the angle between the ith transmitting antenna and the receiving antenna. ϕ_m is the object rotation angle.

Note that the scattered field is received by an antenna on the negative X axis shown in Fig. 1(a). The Fourier-domain data (or $\bar{p}$-space data) contributed from the ith source are then projected on the direction of $\hat{p}_i$. Namely, the source at θ_i contributes a line of Fourier-domain data at $(\theta_i/2)$ as shown in Fig. 1(b), as k_0 is stepped from $k_{\min}$ to $k_{\max}$. In other words, a line of Fourier-domain data lies in the direction of $\hat{p}_i$ with the range from $k_{\min}\cos(\theta_i/2)$ to $k_{\max}\cos(\theta_i/2)$. In order to fill the Fourier-domain space, one can then rotate the scattering object, or equivalently rotate the direction of $\hat{p}_i$ in the Fourier-domain space, to record the scattered field. Fig. 1(c) shows the Fourier-domain acquired at three rotation angles of ϕ_m (i.e., angular diversity technique). It illustrates that an n-fold Fourier-domain can be acquired using n sources in a quasi-monostatic scattering arrangement with the use of illumination diversity technique.

Since the illuminated regions on the scattering object surface contributed from different sources are overlapped as shown in Fig. 1(a), the induced surface currents from each source are then coherently superimposed on the object surface. The scattered field U^s in (10) is therefore a coherent summation of the scattered fields radiated from each illuminated region. In order to relate the reconstructed microwave image to the scattered field given in (10), the corresponding Fourier-domain data contributed from each source has to be extracted. By rewriting the amplitude E_i in (1) as E_{ij} with $i,j = 1\ldots n$, one can expand (10) to be a set of n equations as

$$\begin{aligned}U_1^s &= C_R[E_{11}\tilde{O}_1 + E_{12}\tilde{O}_2 + \cdots + E_{1n}\tilde{O}_n] \\ U_2^s &= C_R[E_{21}\tilde{O}_1 + E_{22}\tilde{O}_2 + \cdots + E_{2n}\tilde{O}_n] \\ &\vdots \\ U_n^s &= C_R[E_{n1}\tilde{O}_1 + E_{n2}\tilde{O}_2 + \cdots + E_{nn}\tilde{O}_n].\end{aligned} \tag{12}$$

In (12), amplitudes of E_{ij} are properly assigned to yield n linearly independent equations and each equation is considered as a measurement state. In other words, during the measurement to be described in Section III, the amplitudes of n sources are properly arranged for a total of n measurement states. Equation (12) can then be expressed as

$$\begin{bmatrix}\tilde{O}_1 \\ \tilde{O}_2 \\ \vdots \\ \tilde{O}_n\end{bmatrix} = \frac{1}{C_R}\begin{bmatrix}E_{11} & E_{12} & \cdots & E_{1n} \\ E_{21} & E_{22} & \cdots & E_{2n} \\ \vdots & \vdots & \ddots & \vdots \\ E_{n1} & E_{n2} & \cdots & E_{nn}\end{bmatrix}^{-1}\begin{bmatrix}U_1^s \\ U_2^s \\ \vdots \\ U_n^s\end{bmatrix}. \tag{13}$$

Equation (13) shows that results of $\tilde{O}_i$ corresponding to the ith source can be extracted from n sets of the scattered field U_j^s with a known nonsingular matrix $[E_{ij}]$. One can use n attenuators to control the n amplitudes of E_{ij} in one measurement state (i.e., each row in $[E_{ij}]$). In addition, the frequency responses of $[E_{ij}]$ attenuators can be measured to obtain the matrix $[E_{ij}]$.

With the use of frequency diversity technique to have k_0 stepped from $k_{\min}$ to $k_{\max}$, n lines of the Fourier-domain data contributed from n sources in the directions of $\hat{p}_i$ with $i = 1\ldots n$ can be extracted from the n sets of recorded scattered field. It is then equivalent to the Fourier-domain data obtained with the use of single-source illumination and angular diversity technique, such as ISAR arrangement, to synthesize the Fourier-domain data distributed in all the directions of $\hat{p}_i$. Therefore, from the scattering object rotation angle ϕ_m and illumination source angle θ_i, one can correctly locate the exacted Fourier-domain data $\tilde{O}_i$ on the Fourier-domain space using (11). It then shows one can acquire the object Fourier-domain data effectively with the use of illumination diversity technique. In Section III, the experimental measurement system and the calibration method to acquire the scattering object Fourier-domain data will be described.

III. Measurement System and Calibration Method

A. Measurement System

Fig. 2 shows the developed experimental microwave imaging system. It has three horn antennas for simultaneously transmitting swept-frequency microwave signals with power levels controlled by three attenuators. The first, second, and third transmitting antennas are located at about 0°, 30° and −30°, respectively. Note, one can increase the number of transmitting antennas as long as their arrangement satisfies the physical optics condition. The receiving horn antenna is at about 0° for collecting the object scattered field. All the transmitting and receiving antennas are in the far-field region. A Hughes 8010H traveling-wave tube amplifier (TWTA) and an Avantek AWT-18 676 low-noise amplifier (LNA) are connected with an Agilent 8722ES network analyzer to provide proper signal amplification. A personal computer is linked to the measurement system for positioner rotation, instrument control, system calibration, and data recording.

In the measurement, the frequency is stepped from 7.5 to 12.5 GHz for 51 frequency points to give $k_{\min} = 1.57$ rad/cm and $k_{\max} = 2.62$ rad/cm. The scattering object is located on a positioner with rotation angles listed in Table I. In each range of rotation angle there are 15 rotation angles. For example, initially $\theta_1 = 0°$, $\theta_2 = 30°$, and $\theta_3 = -30°$ for the first, second, and third transmitting antennas. Hence the corresponding directions of $\hat{p}_1$, $\hat{p}_2$, and $\hat{p}_3$ are at 0°, 15°, and 345°. As the object rotates from 0° to 14°, the angular range of corresponding Fourier-domain data is from 345° to 30° with 45° span angle. Therefore, one can sequentially rotate the scattering object based on the eight ranges given in Table I to synthesize a total of 360° Fourier-domain data with 1° interval. On the other hand, in the ISAR arrangement with only one transmitting antenna, 360 object rotation angles with 1° interval are needed. Therefore, one

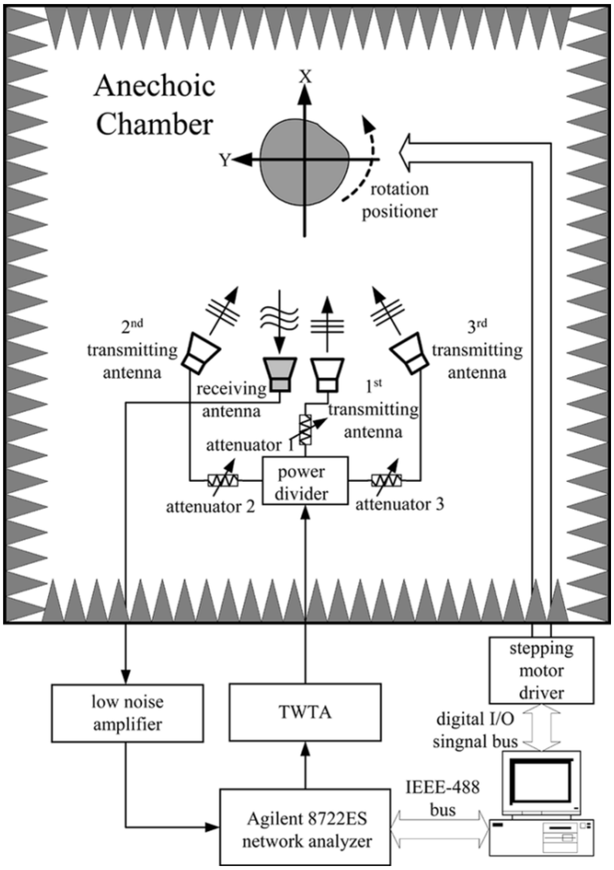

Fig. 2. Automated wide-band quasi-monostatic microwave imaging measurement system using multisource illumination.

TABLE I
RANGE OF SCATTERING OBJECT ROTATION ANGLE AND THE CORRESPONDING ANGULAR RANGE OF OBJECT FOURIER-DOMAIN USING THREE-SOURCE ILLUMINATION

Range of object rotation angle	Angular range of Fourier-domain data
0° — 14°	345° — 30°
45° — 59°	30° — 75°
90° — 104°	75° — 120°
135° — 149°	120° — 165°
180° — 194°	165° — 215°
225° — 239°	215° — 225°
270° — 284°	225° — 300°
315° — 329°	300° — 345°

can effectively reduce the object rotation angles by three times using a three-source arrangement.

In the measurement, the three attenuators are electronically set to the values in Table II corresponding to the three measurement states. One measurement state means to record the frequency-swept object scattered field for one set of attenuator values. The measurement sequence is first to perform three measurement states; then the positioner is rotated to the next object rotation angle for the next three measurement states. After 15 rotation angles, the scattering object is rotated to the next range based on Table I until the end of the rotation. The frequency responses of attenuators are measured before the experiment to calculate $[E_{ij}]^{-1}$ in (13).

TABLE II
ATTENUATOR VALUES FOR THE THREE MEASUREMENT STATES

Measurement State	Attenuator 1	Attenuator 2	Attenuator 3
1st State	**3dB**	0dB	0dB
2nd State	0dB	**3dB**	0dB
3rd State	0dB	0dB	**3dB**

B. Calibration Method

In practice, the measured scattered field can be represented as

$$\left[U_j^m\right] = [I_j] + C_R[E_{ij}][\tilde{O}_i\tilde{R}_j]. \tag{14}$$

I_j is the room clutter term in the jth measurement state. It is the direct measurement without locating any scattering object inside the anechoic chamber. C_R is the range-related term $(-jk_0e^{-jk_0r}/r)$. $[E_{ij}]$ is an $n \times n$ known nonsingular matrix to account for the different complex amplitudes of multi-incident plane waves. $\tilde{O}_i\tilde{R}_j$ is the product of the ith portion of Fourier-domain data and system frequency response in the jth measurement state. Equation (14) can be rewritten as

$$[\tilde{O}_i\tilde{R}_j] = \frac{1}{C_R}[E_{ij}]^{-1}\left\{\left[U_j^m\right] - [I_j]\right\}. \tag{15}$$

For a reference scattering object, (14) becomes

$$\left[U_j^{\mathrm{ref}}\right] = [I_j] + C_R[E_{ij}]\left[\tilde{O}_i^{\mathrm{ref}}\tilde{R}_j\right] \tag{16}$$

where U_j^{ref} is the measured scattered field in the jth measurement state and $\tilde{O}_i^{\mathrm{ref}}$ is the Fourier-domain data of the reference object contributed from the ith transmitting antenna. Equation (16) can be rewritten as

$$\left[\tilde{O}_i^{\mathrm{ref}}\tilde{R}_j\right] = \frac{1}{C_R}[E_{ij}]^{-1}\left\{\left[U_j^{\mathrm{ref}}\right] - [I_j]\right\}. \tag{17}$$

Therefore, the system frequency response of the jth measurement state can be eliminated by dividing $\tilde{O}_i\tilde{R}_j$ in (15) by $\tilde{O}_i^{\mathrm{ref}}\tilde{R}_j$ in (17) to acquire the calibrated ith portion of Fourier-domain data as

$$\tilde{O}_i = \frac{U_j^m - I_j}{U_j^{\mathrm{ref}} - I_j}\tilde{O}_i^{\mathrm{ref}}. \tag{18}$$

Based on the calibration (15), (17), and (18), the calibration and measurement procedures are summarized as the following.

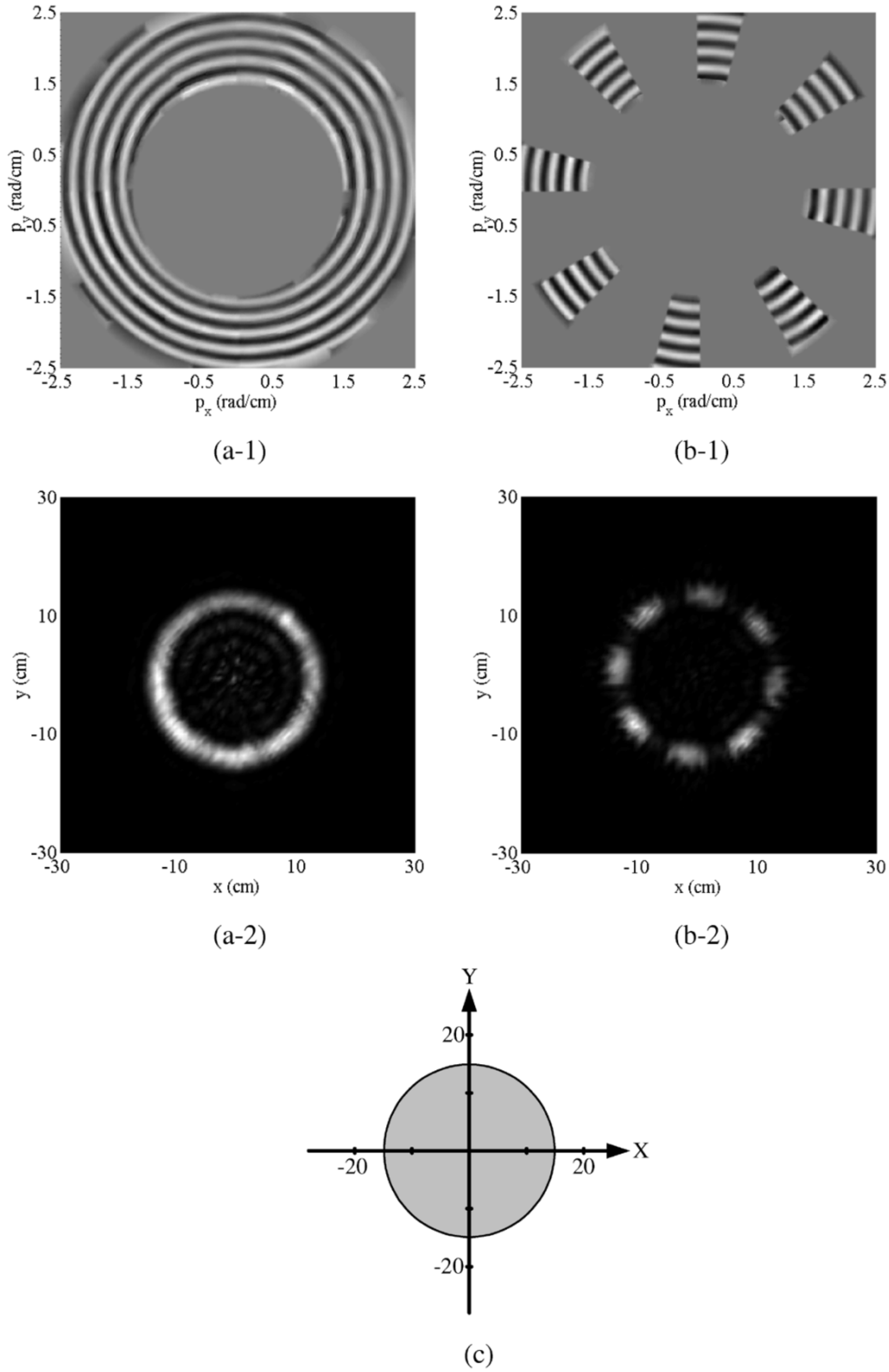

Fig. 3. Measured results of (1) Fourier-domain data and (2) reconstructed images with (a) three-source illumination and (b) single-source illumination of (c) a metallic cylinder with 15 cm radius.

1) Measure the room clutter response for all the measurement states.
2) Position the reference object and measure the quasi-monostatic frequency-swept scattered fields in all measurement states, then subtract room clutter response for each measurement state.
3) Locate the test object and measure the quasi-monostatic frequency-swept scattered fields in all measurement states and at all object rotation angles. Calibrate the object Fourier-domain data using (15), then extract its corresponding Fourier-domain data using (18).
4) Correctly locate all the extracted Fourier-domain data, then use the triangle-based nearest neighbor interpolation method [10] to acquire the object Fourier-domain data in a rectangular format. Finally, perform 2-D inverse fast Fourier transformation to reconstruct the image.

IV. Experimental Results

Based on the above-described measurement system and calibration method, this section presents the experimental results of three different types of scattering objects. They include a

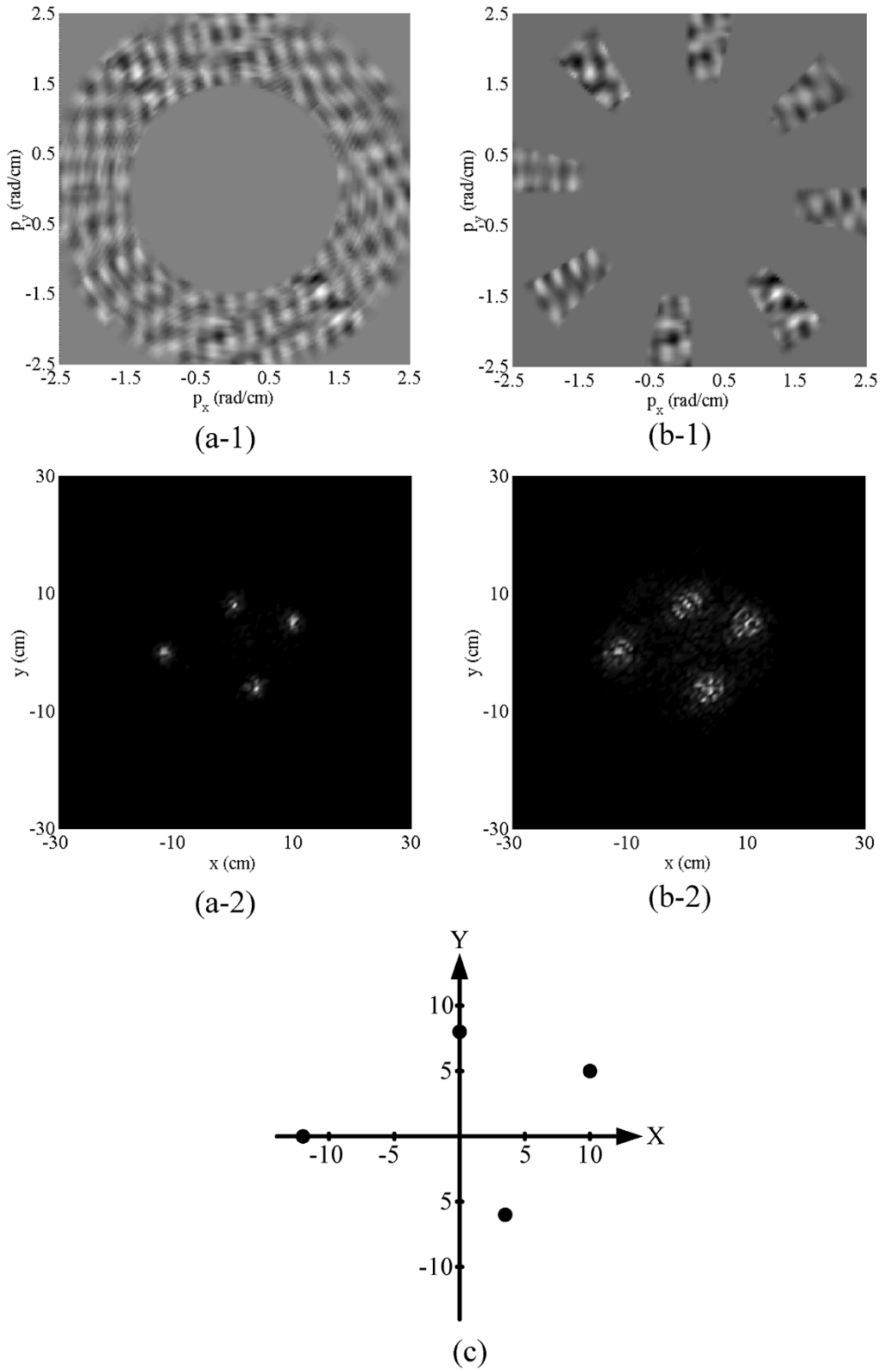

Fig. 4. Measured results of (1) Fourier-domain data and (2) reconstructed images with (a) three-source illumination and (b) single-source illumination of four thin cylinders with (c) geometries at $(-12, 0)$ cm, $(0, 8)$ cm, $(3.5, -6)$ cm, and $(10, 5)$ cm, respectively.

metallic cylinder with 91 cm length and 15 cm radius, four distributed metallic thin cylinders with 113 cm length and 1.5 cm radius acting as discrete line scatterers, and a metal-covered B-52 1:100 scaled model aircraft.

In the three-source measurement arrangement, the scattering object is rotated with a total of 120 object rotation angles listed in Table I to give a total of 360° spanned Fourier-domain data with 1° interval. To illustrate the improvement of image angular resolution, the results using monostatic arrangement acquired at the same rotation angles listed in Table I are also given. A thin metallic cylinder with 113 cm length and 1.5 cm radius is used as a reference object.

For the test object of metallic cylinder with 15 cm radius, the range of ka is 23.6–39.3 rad, hence the measurement is in physical optics regime. The measured Fourier-domain data are shown in Fig. 3(a-1) and (b-1). The measurement with three-source diversity technique gives a 360° spanned Fourier-domain data; however, only a partial Fourier-domain data is

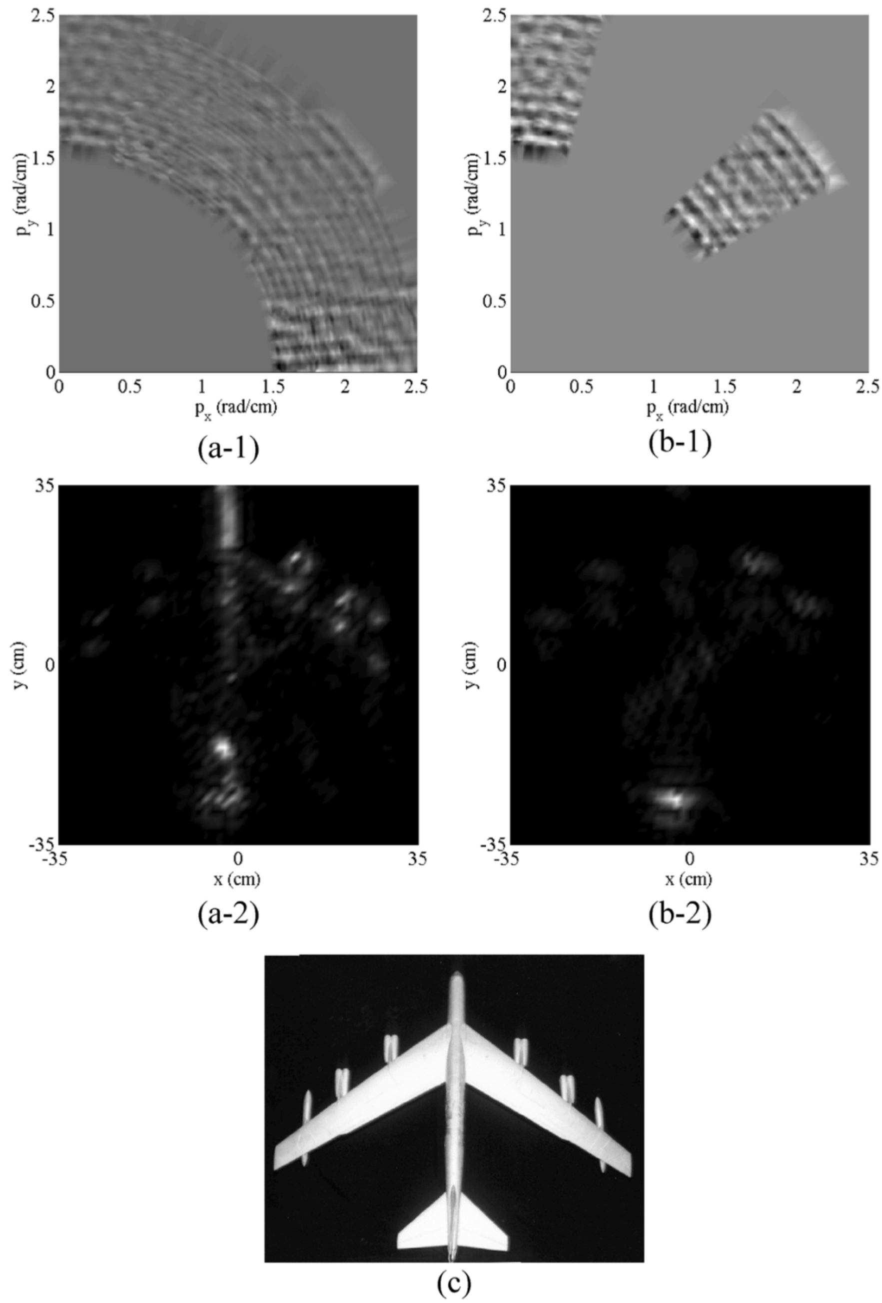

Fig. 5. Measured results of (1) Fourier-domain data and (2) reconstructed images with (a) three-source illumination and (b) single-source illumination of (c) a B-52 1:100 scaled model aircraft.

obtained without using illumination diversity technique. The reconstructed images are shown in Fig. 3(a-2) and (b-2), respectively. A complete circle image is given using three-source illumination, but a fragmental image is obtained without using illumination diversity technique.

For the second type of test object, the range of ka is 2.4–3.9 rad; hence the thin cylinders can be treated as four line scatterers. Measured results of Fourier-domain data and reconstructed image are shown in Fig. 4(a) and (b). The reconstructed image is shown in good agreement with the distribution of four thin cylinders given in Fig. 4(c).

The range of the Fourier-domain data shown in Fig. 4(a-1) for three-source illumination arrangement is about $\Delta p_x = 2$ rad/cm and $\Delta p_y = 2$ rad/cm. The corresponding resolution then gives about 3 cm in both x- and y-directions. However, the area of the Fourier-domain data shown in Fig. 4(b-1) for single source illumination case is one-third of that in Fig. 4(a-1); hence its resolution is about three times worse in x- and y-directions as shown in Fig. 4(b-2). Therefore, for the same object rotation angles, the quasi-monostatic frequency-swept microwave imaging system using illumination diversity technique is shown to be an efficient approach to giving better resolution in comparison with the single source (or ISAR) approach.

For the third test object, a B-52 scaled aircraft, it consists of continuous and discrete scattering centers. The Fourier-domain data for three-source illumination and single source illumination are shown in Fig. 5(a-1) and (b-1). From the reconstructed image shown in Fig. 5(a-2), one can clearly identify the wing, two twin-engines, and the cockpit and tear of the aircraft, but only indistinct images are shown in Fig. 5(b-2) using single source illumination.

V. Conclusion

The basic principle, measurement system, and calibration method for the frequency-swept microwave imaging of perfectly conducting objects using illumination diversity technique are presented in this paper. In Section II, the image reconstruction formulas are developed to acquire the Fourier-domain data for image reconstruction in the situation that the scattering object is under multisource illumination. It proves the linear dependence of the number of sources and the angular resolution of the reconstructed image under the physical optics approximation. In other words, as n sources are properly arranged to fulfill the physical optics approximation, one can reduce the object rotation angle by a factor of n or equivalently improve the angular resolution by a factor of n as compared with ISAR arrangement. Shown in Section IV, the reconstructed images of three types of scattering objects experimentally demonstrate that the developed illumination diversity technique can effectively synthesize the Fourier-domain data in angular directions. In addition, this technique can be applied to the multistatic microwave imaging by simultaneously using multisource illumination and multiple coherent receivers. This will then further improve the image resolution and imply the feasibility of a real-time microwave imaging system. Another interesting application of illumination diversity technique is its capable imaging of stealthy type objects whose radar cross-section is usually minimized only for certain incident illumination and observation angles. Therefore, multiple sources operated simultaneously provide a practical solution.

References

[1] R. M. Lewis, "Physical optics inverse diffraction," *IEEE Trans. Antennas Propag.*, vol. AP-24, no. 3, pp. 308–314, May 1969.

[2] N. N. Bojarski, "A survey of physical optics inverse scattering indentity," *IEEE Trans. Antennas Propag.*, vol. AP-30, no. 5, pp. 980–989, Sep. 1982.

[3] N. H. Farhat, C. L. Werner, and T. H. Chu, "Prospects for there-dimensional projective and tomographic imaging radar networks," *Radio Sci.*, vol. 19, pp. 1347–1355, Sep.–Oct. 1984.

[4] T. H. Chu and D. B. Lin, "On microwave imagery using Bojarski's identity," *IEEE Trans. Microwave Theory Tech.*, vol. 37, no. 7, pp. 1141–1144, Jul. 1989.

[5] D. L. Mensa, *High Resolution Radar Imaging*. Dedham, MA: Artech House, 1981.

[6] R. F. Harrington, "On scattering by large conducting bodies," *IRE Trans. Antennas Propag.*, vol. AP-6, no. 2, pp. 150–153, Apr. 1957.

[7] ——, *Time-Harmonic Electromagnetic Fields*. New York: McGraw-Hill, 1961.

[8] C. K. Chen and N. H. Farhat, "Frequency swept tomographic imaging of three-dimensional perfectly conducting objects," *IEEE Trans. Antennas Propag.*, vol. 29, no. 2, pp. 312–319, Mar. 1981.

[9] F. C. Chen and W. C. Chew, "Time-domain ultra-wideband microwave imaging radar," in *Proc. IEEE Instrumentation Measurement Technology Conf.*, St. Paul, MN, May 18–21, 1998, pp. 648–650.

[10] *MATLAB: The Language of Technical Computing*. Natick, MA: MathWorks, 1996.

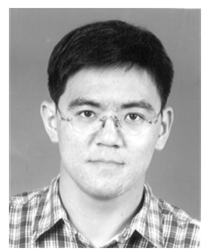

Chao-Hsiung Tseng (S'03–M'05) was born in Miaoli, Taiwan, R.O.C., on July 4, 1974. He graduated in electronic engineering from National Taipei Institute of Technology, Taipei, Taiwan, R.O.C., in 1994 and received the M.S. and Ph.D. degrees in communication engineering from National Taiwan University, in 1999 and 2004, respectively.

From 1999 to 2000, he was an Associate Researcher at the Center for Measurement Standards, Industrial Technology Research Institute, Hsinchu, Taiwan, R.O.C. He is currently a Postdoctoral Research Fellow with the Department of Electrical Engineering, National Taiwan University. His research interests include microwave-imaging systems and techniques, microwave measurements, and calibration techniques.

Tah-Hsiung Chu (M'87) received the B.S. degree from National Taiwan University, Taipei, Taiwan, R.O.C., in 1976 and the M.S. and Ph.D. degrees from the University of Pennsylvania, Philadelphia, in 1980 and 1983, respectively, all in electrical engineering.

From 1983 to 1986, he was a Member of Technical Staff with the Microwave Technology Center, RCA David Sarnoff Research Center, Princeton, NJ. Since 1986, he has been on the Faculty of the Department of Electrical Engineering, National Taiwan University, where he is now a Professor of electrical engineering. His research interests include microwave-imaging systems and techniques, microwave circuits and subsystems, microwave measurements, and calibration techniques.